

Gain Scheduled Attitude Control of Fixed-Wing UAV With Automatic Controller Tuning

Pakorn Poksawat, Liuping Wang, and Abdulghani Mohamed

Abstract—Fixed-wing unmanned aerial vehicles (UAVs) have become increasingly important in military, civil, and scientific sectors. Because of the existing nonlinearities, effective control of this type of UAV remains a challenge. This paper proposes a gain scheduled proportional–integral derivative (PID) control system for fixed-wing UAVs where a family of PID cascade control systems is designed for several operating conditions of airspeed. This is done using an automatic tuning algorithm, where the controllers are automatically selected by deploying an airspeed sensor positioned ahead of the aircraft. Furthermore, the actual gain scheduling is carried out by forming an interpolation between the family members of the linear closed-loop system, which ensures a smooth transition from one operating point to another. Experimental results are conducted in a wind tunnel to show the successful design and implementation of the gain scheduled control system for the fixed-wing UAV and the significant performance improvement over a linear control system without controller adaptation.

Index Terms—Autotuner, fixed-wing unmanned aerial vehicle (UAV), gain scheduled control system, proportional–integral derivative (PID) controller.

I. INTRODUCTION

RECENTLY, fixed-wing unmanned aerial vehicles (UAVs) have become a feasible solution for many applications in military, civil, and scientific sectors [1], [2], including surveillance, localization, and mapping. UAVs will routinely operate in urban environments for a range of applications and around large infrastructure for data gathering or spling extending range and endurance [3]–[5]. Due to the nature of fixed-wing aircraft's nonlinear dynamics, a robust control system is required in order to achieve stable flights in most outdoor conditions [6]–[8]. Although there are many advances in control algorithms, such as model predictive control, adaptive control, and sliding mode control, they are computationally demanding and unsuitable for small scale embedded processors in UAV avionics [9].

One of the most commonly used controllers in autopilots is proportional–integral derivative (PID) because of the implementation simplicity and low computational intensity [10], [11]. However, the drawback of this type of linear controller is that it may not be able to satisfy the design

Manuscript received January 30, 2017; accepted May 7, 2017. Date of publication June 20, 2017; date of current version June 11, 2018. Manuscript received in final form May 22, 2017. Recommended by Associate Editor L. Fagiano (*Corresponding author: Liuping Wang*.)

The authors are with RMIT University, Melbourne, VIC 3001, Australia (e-mail: liuping.wang@rmit.edu.au).

Color versions of one or more of the figures in this paper are available online at <http://ieeexplore.ieee.org>.

Digital Object Identifier 10.1109/TCST.2017.2709274

requirements for a wide range of operational conditions. To solve this issue, gain scheduling approaches have been utilized for fixed-wing aircraft [12]–[14]. The main advantages of gain scheduled PID controllers are that they are able to maintain stability in varying operating conditions while maintaining simplicity in the implementation [15].

The design and tuning procedures of a gain scheduled controller for an aircraft require the mathematical model of the vehicle's dynamics with physical parameters that can be estimated from system identification or via wind tunnel experiments [16]. The common practice in selecting the controller parameters predominantly involves the utility of nonlinear simulation models [17]. Followed by experiments performed during flight while maintaining communication with the engineer who can tune the flight controller's parameters. These methods can be time-consuming and difficult to control for the flight test pilots [18]. In addition, there are several issues associated with the process of tuning gain scheduled controllers for nonlinear systems. First, it is often a trial-by-error approach to design a gain scheduled control system due to the measurement errors of the physical parameters. Second, the actuator and sensor dynamics are often neglected in the nonlinear mathematical model. Third, the physical parameters may vary with respect to the operating conditions. Finally, fixed-wing UAVs require cascade control system structures, which further complicates the tuning procedures that can potentially increase cost and workload for the designers [18]–[20].

In our recent work [21], an automatic tuning algorithm has been used for the controller design of a microaircraft. However, because of the existing nonlinearities in fixed-wing UAVs, the PID controllers tuned for one operating condition are found to give severe oscillations when the airspeed changes. This motivates us to investigate gain scheduled PID control of fixed-wing unmanned aircraft. In the past, automatic tuning of PID controllers using relay feedback control has been extensively studied [22]–[28]. However, gain scheduled PID controller design using relay feedback has not been explored.

This paper, therefore, proposes the use of relay feedback test to automate the gain scheduled controller design procedures. There are several new contributions made in relation to gain scheduled PID controller design and implementation for fixed-wing UAVs. Differing from the traditional way of designing gain scheduled PID controllers, the proposed method will automatically find a family of PI controller parameters through wind tunnel experiments under relay feedback control in which the actuator and sensor dynamics have been effectively considered. Through choice of weighting parameters, the gain

scheduled control signal is expressed in an incremental form, with an antiwindup mechanism, similar to that used in the formulation of a model predictive controller [29], [30]. This naturally leads to a bumpless transfer mechanism, which is required when switching from one operational condition to another. Finally, a sensor is used to measure the airspeed in advance to enable the scheduler to correctly identify the particular linear PI controller associated with the operating conditions. All the contributions have been validated with wind tunnel flight tests using a custom developed flight controller board. Additionally, a simulation study has been performed to compare the proposed method with the conventional model-based design approach [31], which highlights its advantages in overcoming unknown actuator dynamics and the unnecessary to have the model information. It is envisaged that the same design method can be adapted to any type of fixed-wing UAV systems, which, in general, automates the control system design for gain scheduled controllers.

This paper is outlined as follows. In Section II, the mathematical model is presented to motivate selection of the gain scheduled controller structure. The design and the implementation of the gain scheduled controller using autotuner are explained in Section III. In Section IV, the tuning procedures are presented with experimental results from the wind tunnel. Finally, comparative studies have been performed to show the improved performance over a linear control system without adaptation in Section V.

II. GAIN SCHEDULED CONTROL SYSTEM STRUCTURE

To motivate the need of a gain scheduled PID control system, the physical model of a conventional fixed-wing UAV is discussed first in this section.

A. Nonlinear Attitude Model of Fixed-Wing UAV

As shown in [31] and [32], the attitude dynamics of a fixed-wing UAV are described by the following differential equations:

$$\begin{bmatrix} \dot{p} \\ \dot{q} \\ \dot{r} \end{bmatrix} = \begin{bmatrix} \Gamma_1 pq - \Gamma_2 qr \\ \Gamma_5 pr - \Gamma_6(p^2 - r^2) \\ \Gamma_7 pq - \Gamma_1 qr \end{bmatrix} + \begin{bmatrix} \Gamma_3 L + \Gamma_4 N \\ \frac{1}{I_y} M \\ \Gamma_4 L + \Gamma_8 N \end{bmatrix} \quad (1)$$

where p , q , and r are roll, pitch, and yaw angular rates in the body frame. L , M , and N are the moments about roll, pitch, and yaw axes, respectively. I_x , I_y , and I_z are the moment of inertia about x , y , and z axes, while I_{xz} is the product moment of inertia. Furthermore, the following constants in the mathematical model (1) are calculated according to the following relations:

$$\begin{aligned} \Gamma_1 &= \frac{I_{xz}(I_x - I_y + I_z)}{\Gamma}, & \Gamma_2 &= \frac{I_z(I_z - I_y) + I_{xz}^2}{\Gamma} \\ \Gamma_3 &= \frac{I_z}{\Gamma}, & \Gamma_4 &= \frac{I_{xz}}{\Gamma}, & \Gamma_5 &= \frac{I_z - I_x}{I_y} \\ \Gamma_6 &= \frac{I_{xz}}{I_y}, & \Gamma_7 &= \frac{(I_x - I_y)I_x + I_{xz}^2}{\Gamma}, & \Gamma_8 &= \frac{I_x}{\Gamma} \end{aligned}$$

and

$$\Gamma = I_x I_z - I_{xz}^2.$$

For control system design, the dynamics equations used to describe the attitude of the aircraft are related to the control surfaces ailerons, elevator, and rudder denoted as δ_a , δ_e , and δ_r , respectively. To this end, the aerodynamic moments are modeled as follows:

$$\begin{aligned} L &= L(p, r, \delta_a, \delta_r) = \ell_p p + \ell_r r + \ell_{\delta_a} \delta_a + \ell_{\delta_r} \delta_r \\ M &= M(q, \delta_e, \delta_t) = m_q q + m_{\delta_e} \delta_e + m_{\delta_t} \delta_t \\ N &= N(p, r, \delta_a, \delta_r) = n_p p + n_r r + n_{\delta_a} \delta_a + n_{\delta_r} \delta_r \end{aligned} \quad (2)$$

where ℓ , m , and n are the force coefficients for the roll, pitch, and yaw axes, respectively. The mathematical equations can be rewritten in terms of the manipulated control variables δ_a , δ_e , and δ_r with the following forms:

$$\begin{aligned} \dot{p} &= \Gamma_1 pq - \Gamma_2 qr + \frac{1}{2} \rho V_a^2 S b \\ &\times \left[C_{\ell_0} + C_{\ell_{\beta_C}} \beta_C + C_{\ell_p} \frac{bp}{2V_a} + C_{\ell_r} \frac{br}{2V_a} \right. \\ &\left. + C_{\ell_{\delta_a}} \delta_a + C_{\ell_{\delta_r}} \delta_r \right] \end{aligned} \quad (3)$$

$$\begin{aligned} \dot{q} &= \Gamma_5 pr - \Gamma_6(p^2 - r^2) + \frac{\rho V_a^2 S c}{2I_y} \\ &\times \left[C_{m_0} + C_{m_a} + C_{m_q} \frac{cq}{2V_a} + C_{m_{\delta_e}} \delta_e \right] \end{aligned} \quad (4)$$

$$\begin{aligned} \dot{r} &= \Gamma_7 pq - \Gamma_1 qr + \frac{1}{2} \rho V_a^2 S b \\ &\times \left[C_{n_0} + C_{n_{\beta_C}} \beta_C + C_{n_p} \frac{bp}{2V_a} + C_{n_r} \frac{br}{2V_a} \right. \\ &\left. + C_{n_{\delta_a}} \delta_a + C_{n_{\delta_r}} \delta_r \right] \end{aligned} \quad (5)$$

where C_{xy} denotes the aerodynamics derivative coefficient for a given x_y , ρ is the air density, V_a is the airspeed, S is the wing platform area, b is the wingspan of the airframe, c is the mean chord of the wing, and β_C is the course angle.

The relationships between the body frame angular rates and the Euler angular rates are described in the following equation:

$$\begin{bmatrix} \dot{\phi} \\ \dot{\theta} \\ \dot{\psi} \end{bmatrix} = \begin{bmatrix} 1 & \sin(\phi)\tan(\theta) & \cos(\phi)\tan(\theta) \\ 0 & \cos(\phi) & -\sin(\phi) \\ 0 & \sin(\phi)\sec(\theta) & \cos(\phi)\sec(\theta) \end{bmatrix} \begin{bmatrix} p \\ q \\ r \end{bmatrix} \quad (6)$$

where $\dot{\phi}$, $\dot{\theta}$, and $\dot{\psi}$ are roll, pitch, and yaw angular rates in the Euler frame.

B. Overview of the Gain Scheduled Control System

Although the mathematical model and the design framework are presented for the three axes, for simplicity, only the roll axis controller is considered. This means that we will only consider the dynamic equation (3) together with the first row of (6). First, (3) shows that there are two bilinear relationships between p and q as well as q and r . However, because angular body rates (p , q , and r) are under closed-loop feedback control, in a normal operation, it is assumed

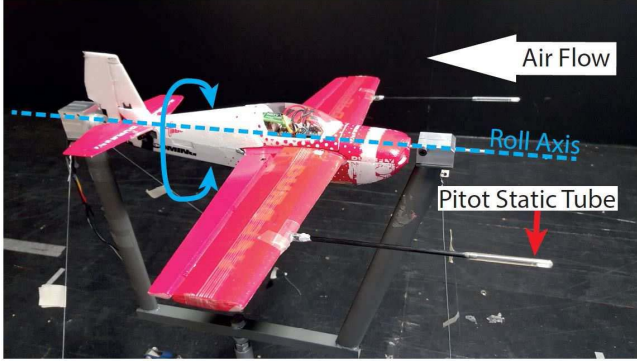


Fig. 1. Roll rig experimental setup.

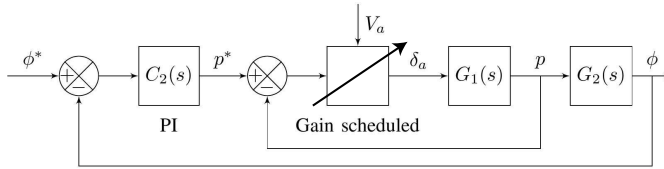


Fig. 2. Cascaded gain scheduled PI control system diagram.

that their values are close to zero; hence, the variations of the bilinear terms do not have significant impact on the closed-loop stability and performance. In contrast, the airspeed V_a^2 term is not controlled and can change depending on the flight path and weather conditions. The variation of the airspeed will have a significant impact on the closed-loop stability and performance, meaning that a PID controller designed for a given airspeed V_a may become unstable if the airspeed changes. Therefore, the airspeed V_a is selected as the operating condition identifier.

In the design and implementation of the gain scheduled control system, the parameter used to identify the operating conditions of the system is required to be measured in real time. In this application, an aircraft equipped with airspeed sensors is used, as shown in Fig. 1. Although only one of the sensors is used, another sensor is installed for increased redundancy. The differential pressure sensors and pitot static tubes are used to measure the airspeed in advance, because they are positioned ahead of the aircraft. The advanced measurement of the airspeed is advantageous in providing phase-advanced information relating to the changes in operating conditions, leading to smoother transitions from one operating condition to another.

For the roll axis control, the primary control surface used to influence the angular rate, p , is the aileron deflection, δ_a , which is the control variable in this case. The control objective is that for a given reference signal ϕ^* , the roll angle ϕ will follow its reference while rejecting disturbances. To meet these objectives, the closed-loop control system for the roll axis is configured as a cascaded structure shown in Fig. 2, where the inner loop has a gain scheduled controller and $C_2(s)$ is the controller for the outer loop. The measurement of airspeed V_a will determine which PI controller will be used in the inner-loop control system. The outer-loop PI controller is less

sensitive to the variation of the airspeed because of the inner-loop feedback control; thus, gain scheduling on the outer loop is not required. Experimental validations later will confirm this is indeed the case.

III. DESIGN AND IMPLEMENTATION OF GAIN SCHEDULED PID CONTROLLER

A typical gain scheduled PID control system design procedure for nonlinear plants involves the selection of several operating points to cover the whole range of the plant's operation. At each selected operating point, a PID control system is designed off-line before the commission of a gain scheduled control system. When the gain scheduled control system is in operation, the identifier, which is the sensing device for airspeed in this application, will provide the plant operating information in real time. With the sensed plant operating information, a PID controller from the off-line design is automatically selected and commissioned in real time. When the operating condition changes, another corresponding PID controller automatically takes over.

There are three remaining tasks that are required to be further addressed in the successful design and implementation of a gain scheduled control system. First, a family of PID controllers will be designed at each operating point to provide a stable closed-loop system with desired performance. Second, the actual gain scheduling will be carried out by forming an interpolation between the family members of the linear closed-loop system, which will ensure a smooth transition from one operating point to another. Third, because the gain scheduled control system uses linear control strategies to control a nonlinear system, its closed-loop stability is established using the slow time variation theory proposed in [33]; hence, its validation becomes an important task.

A. Automatic Tuning of Cascade PI Controllers

The design of a family of PID controllers can be performed either using the physical model given in (3) and (6) or using the automatic tuning procedure proposed in the following. The automatic tuning procedure will not only take into consideration of the effect of nonlinearity in the selection of the controller parameters, but also the actuator dynamics. The autotuning algorithm has been used in the authors' previous work [21] where a single operating condition was considered. For completion of this paper, this algorithm is briefly summarized as follows.

The first step is to conduct identification experiment under relay feedback control in the wind tunnel with a given airspeed V_a . Because it is a cascade control system, the inner-loop control PI system is automatically tuned first. Once the inner-loop PI controller is found, the autotuning process is repeated to find the outer-loop controller. Since the variation of q is around 0 in the testing environment, the inner-loop system is modeled as an integrator with time delay, where the time delay is predominantly caused by the actuator dynamics. Thus, in the relay feedback control experiment, a proportional controller K_T is used to stabilize the system to ensure the safety of the aircraft. As an illustration, Fig. 3 shows the setup

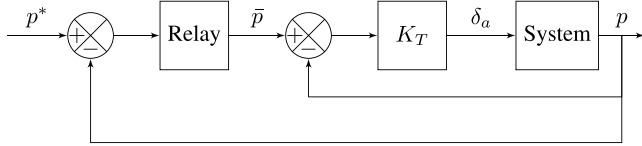


Fig. 3. Relay feedback control system structure for the inner loop.

of the relay feedback control system for roll angular rate p in body frame.

After the relay feedback control experiment, the experimental data for the relay control signal \bar{p} and the output signal p are collected. Then, either Fourier transform analysis or frequency sampling filter-based modeling technique [34] can be used to find the closed-loop frequency response $T(e^{j\omega})$, followed by the calculation of open-loop frequency response $G(j\omega)$, where:

$$G(e^{j\omega}) = \frac{1}{K_T} \frac{T(e^{j\omega})}{1 - T(e^{j\omega})} \quad (7)$$

where $\omega = (2\pi/T)$ and T is the period of the oscillation.

Assume that the inner-loop system is described by an integrator plus delay model in the following form:

$$G(s) = \frac{K_p e^{-ds}}{s}. \quad (8)$$

The parameters K_p and d can be easily calculated using the following equations:

$$K_p = \omega |G(j\omega)| \quad (9)$$

and

$$d = -\frac{1}{\omega} \tan^{-1} \frac{\text{Imag}(jG(j\omega))}{\text{Real}(jG(j\omega))}. \quad (10)$$

Upon obtaining the integrator plus time delay model, the PID controller parameters are calculated using the tuning rules presented in [34] and [35]. The set of tuning rules presented has the characteristics of being simple with gain and phase margins conveniently given. With the tuning rules, the PID controller parameters are calculated using the following normalized parameters:

$$\begin{aligned} K_c &= \frac{\hat{K}_c}{dK_p} \\ \tau_I &= d\hat{\tau}_I \\ \tau_D &= d\hat{\tau}_D. \end{aligned}$$

For damping coefficient $\xi = 1$, the normalized PID controller parameters are calculated as

$$\hat{K}_c = \frac{1}{0.5080\beta + 0.6208} \quad (11)$$

$$\hat{\tau}_I = 1.9885\beta + 1.2235 \quad (12)$$

$$\hat{\tau}_D = \frac{1}{1.0043\beta + 1.8194} \quad (13)$$

where the parameter β is the scaling factor for the desired closed-loop time constant, which is defined as

$$\tau_{cl} = \beta d.$$

The user can select the value of β corresponding to the desired closed-loop time constant, but also the gain margin and the phase margin for the closed-loop system [34]. This set of tuning rules for integrating systems has been independently evaluated in [28].

B. Gain Scheduled PI Controller

In this application, three sets of PI controller parameters are automatically found, namely: low, medium, and high airspeeds. For notational simplicity, let K_c^L and τ_I^L denote the PI controller parameters corresponding to the low airspeed V_a^L , K_c^M and τ_I^M the medium airspeed V_a^M , and K_c^H and τ_I^H the high airspeed V_a^H .

The interpolation between the family members of the PI controllers is realized through the computation of the derivative of the control signal $\dot{u}(t)$

$$\begin{aligned} \dot{u}(t) = & \lambda^L \left(K_c^L \dot{e}(t) + \frac{K_c^L}{\tau_I^L} e(t) \right) + \lambda^M \left(K_c^M \dot{e}(t) + \frac{K_c^M}{\tau_I^M} e(t) \right) \\ & + \lambda^H \left(K_c^H \dot{e}(t) + \frac{K_c^H}{\tau_I^H} e(t) \right) \end{aligned} \quad (14)$$

where $e(t) = p^*(t) - p(t)$ is the actual feedback error in the PI control system and the parameters λ^L , λ^M , and λ^H are the weighting parameters. They are valued between 0 and 1, and calculated according to the measured airspeed. At any given instance, they are summed up to 1. To ensure smooth transition, a band $\pm\delta$ is used for the medium airspeed. More specifically, the weighting parameters λ^L , λ^M , and λ^H are calculated as

- 1) If $V_a(t) \leq V_a^L$
 $\lambda^L = 1$, $\lambda^M = 0$, $\lambda^H = 0$.
- 2) If $V_a^M - \delta \leq V_a(t) \leq V_a^M + \delta$
 $\lambda^L = 0$, $\lambda^M = 1$, $\lambda^H = 0$.
- 3) If $V_a(t) \geq V_a^H$
 $\lambda^L = 0$, $\lambda^M = 0$, $\lambda^H = 1$.

When the airspeed is outside of the three bands, a combination of the two controllers from the two closest regions are used. For instance, assuming that the operating condition is between the high and medium speed band ($V_a^M + \delta < V_a(t) < V_a^H$), the parameter λ^H and λ^M are defined as a function of $V_a(t)$ as

$$\lambda^H = \frac{V_a(t) - V_a^H - \delta}{V_a^H - V_a^M - 2\delta}; \quad \lambda^M = 1 - \lambda^H; \quad \lambda^L = 0.$$

For clarity, Fig. 4 shows how the weighting parameters are calculated based on the identifier of the operating condition.

The calculation of the control signal requires the discretization of (14). Assume that the sampling interval is defined as $\Delta t = t_i - t_{i-1}$, where t_i is the current sampling time and t_{i-1} is the past sampling time. At the sampling time t_i , by approximating $\dot{u}(t_i) \approx (u(t_i) - u(t_{i-1})/\Delta t)$ and $\dot{e}(t_i) \approx (e(t_i) - e(t_{i-1})/\Delta t)$, the continuous-time control law given by (14) is expressed in the corresponding

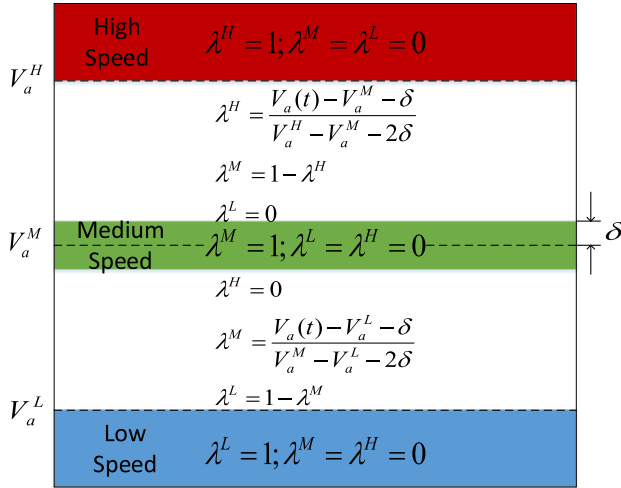


Fig. 4. Weighting parameters interpolation diagram.

discrete-time form

$$\begin{aligned} u(t_i) = & u(t_{i-1}) \\ & + \Delta t \left\{ \lambda^L \left(K_c^L (e(t_i) - e(t_{i-1})) + \frac{K_c^L}{\tau_I^L} e(t_i) \Delta t \right) \right. \\ & + \lambda^M \left(K_c^M (e(t_i) - e(t_{i-1})) + \frac{K_c^M}{\tau_I^M} e(t_i) \Delta t \right) \\ & \left. + \lambda^H \left(K_c^H (e(t_i) - e(t_{i-1})) + \frac{K_c^H}{\tau_I^H} e(t_i) \Delta t \right) \right\}. \end{aligned} \quad (15)$$

Note that the computation of the discretized control signal at the sampling instant t_i uses the past sample of control signal. This iterative calculation will not require the steady-state value of the control signal. It, hence, not only simplifies the controller implementation procedure, but also naturally provides a mechanism for bumpless transfer from one operating condition to another. This type of approaches has been used in the past for the implementation of gain scheduled model predictive controllers [30]. An additional advantage of the gain scheduled control law is that an antiwindup mechanism can be readily added with a minor modification. More specifically, in the antiwindup implementation, the control signal is first calculated using (15) and denoted by $\bar{u}(t_i)$, followed by evaluating whether the constraints have been violated and choosing the actual control signal value:

$$u(t_i) = \begin{cases} u_{\min} & \bar{u}(t_i) < u_{\min} \\ \bar{u}(t_i) & u_{\min} \leq \bar{u}(t_i) \leq u_{\max} \\ u_{\max} & \bar{u}(t_i) > u_{\max} \end{cases} \quad (16)$$

where u_{\max} and u_{\min} are the maximum and minimum control signals, respectively. This antiwindup mechanism has been validated on PID control of electrical drives and power converters [30].

IV. AUTOMATIC CONTROLLER TUNING

To evaluate the proposed algorithm, experimental results are presented in this section. First, the experimental setup

TABLE I
FIXED-WING UAV SPECIFICATIONS

Description	Details
Airframe	Slick 360
Airfoil	NACA0012
Wing span	0.490m
Fuselage length	0.421m
Wing area	0.44m ²
Average chord	0.0885m
Weight	130g
Cruise speed	10m/s

TABLE II
CUSTOM DEVELOPED FLIGHT CONTROLLER SPECIFICATIONS

Component	Model
Microprocessor	MK20DX256 (72 MHz Cortex-M4)
Inertial measurement unit	MPU6050
RC receiver	OrangeRX R615X 2.4 Ghz receiver
RC transmitter	Turnigy 9XR PRO radio transmitter
datalogger	CleanFlight blackbox data logger
servos	HK-5330 Ultra-micro servo
Electronic speed controller	Turnigy Multistar 10A ESC
Brushless DC Motor	NTM prop drive 13-12 2600 KV

is described, followed by a feedback relay experiment on the inner and outer loop systems at different operating conditions to obtain the appropriate controller gains.

A. Experimental Setup

The fixed-wing aircraft chosen for this paper is the Slick 360 airframe, and its operational speed is between 7 and 15 m/s (see Fig. 1) [36]. The aircraft's physical specifications are described in Table I [37]. In order to individually isolate the roll axis, the aircraft is fixed along its thrust line on the roll test rig. The roll axis is allowed to rotate freely with minimal friction, while the pitch and yaw axes are fixed and cannot be rotated. This ensures that the roll axis will not be affected by the changes in other axes. The aircraft was installed on the rig at 0° angle-of-attack.

For this experimental study, a custom developed flight controller is used. The avionic and flight controller components are shown in Table II.

A pitot static tube is connected to a differential pressure sensor to measure the airspeed, and the information is used for real-time gain scheduling. The tube is 15 cm in length and the cruise speed of the aircraft is 10 m/s; thus, the airspeed is sensed approximately 15 ms prior to reaching the leading edge of the wing. Furthermore, the custom developed flight controller has a control loop sampling rate of $\Delta t = 5$ ms, which is faster than the time-advantage. This means that once the change in airspeed is detected, the flight controller is able to schedule the controller's parameters in advance. The advantage of implementing this sensing technique is that there is sufficient time to prepare for the change in airspeed rather

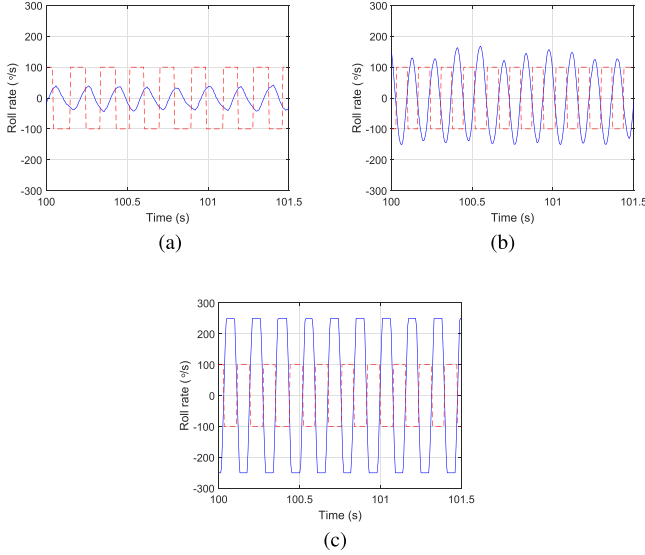


Fig. 5. Inner loop relay results. Dashed lines: relay reference. Solid lines: roll rate feedback. (a) Minimum flight speed (7 m/s). (b) Operational cruise speed (10 m/s). (c) Maximum flight speed (15 m/s).

than correcting for the angular displacement after the aircraft inertial response has already been effected [38].

In order to have a fair comparison between different control strategies, repeatable experimental conditions are imperative. Wind tunnel environments provide us with an ideal testing environment as the wind speed can be adjusted to replicate different airspeeds. It is more preferable than outdoor flights due to the repeatability concerns associated with varying weather conditions, in addition to eliminating the risk of crashing during the tests. The wind tunnel utilized has a $2 \times 3 \times 9 \text{ m}^3$ test section and has been demonstrated to be sufficient at replicating outdoor flight conditions [37], where its attributes are described in [39].

B. Inner Loop Relay Experiment

A proportional controller is chosen as $K_{T_1} = 0.3$. The amplitude of the relay reference signal is selected as $100^\circ/\text{s}$, which is within the flight envelope of the UAV, so that the experiment yields practical results. In order to prevent gyroscope noise from affecting the experimental results, the hysteresis of $30^\circ/\text{s}$ is selected to prevent the relay switching from measurement noise. In order to demonstrate the existing nonlinearity that affects the dynamics of the inner loop system, three relay feedback experiments were conducted separately at 7-, 10-, and 15-m/s flight speed. The results are presented in Fig. 5(a)–(c), respectively. It is seen from Fig. 5(a)–(c) that despite the same relay amplitude used in the experiments, the output responses clearly have different amplitudes, as expected due to the nonlinearities.

The estimated inner loop steady-state gain K_p and estimated time delay d were found and shown in Table III. It is seen from Table III that the mathematical model obtained at the lower airspeed has the smallest time delay and gain. As the airspeed increases, both time delay and gain have increased significantly where, in particular, the time delay has increased in twofold and the gain in threefold.

TABLE III
RESULTS FROM THE RELAY EXPERIMENT

	K_p	d
Low speed	24.918	0.0238
Medium speed	65.51	0.0364
High speed	76.886	0.0446

TABLE IV
IDENTIFIED INNER LOOP CONTROLLER PARAMETERS

	K_c	τ_I
Low speed	0.92	0.095
Medium speed	0.23	0.146
High speed	0.16	0.178

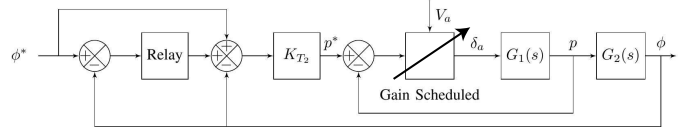


Fig. 6. Outer loop relay feedback structure.

The closed-loop time constant is specified by selecting the performance factor β , based on the desired gain and phase margins [34]. Higher performance factor β results in slower closed-loop system response and vice versa. For a cascade control structure, it is vital for the inner loop system response to be very fast. Hence, β is chosen as 2, leading to approximately two gain margin and 40° phase margin. While keeping the performance factor the same for all three sets of experiments, the identified controller gains are calculated and presented in Table IV.

Based on the dynamics equations, planes require less actuation and when traveling at higher speed, lower controller gains are needed. On the other hand, the control surface deflections need to be higher at low speed; thus, higher gains are more desirable. It is seen that the identified controller gains, in Table IV, decrease as the airspeed increases. This shows that the tuning algorithm can automatically provide designers' appropriate controller's parameters at varying operating conditions.

C. Outer Loop Relay Experiment

Once the inner loop has been tuned at each of the operating points, the relay experiment was conducted on the outer loop. The feedback relay control structure is as shown in Fig. 6, where the inner loop controller is the gain scheduled PI controller implemented with parameters from Table IV. Based on the same design procedure as the inner loop, the relay parameters are chosen as follows, $K_{T_2} = 3$, a relay amplitude of 20° , and a hysteresis of 10° .

Fig. 7 presents the results of the feedback relay experiment at the three operating regions. It is clearly seen that for the outer loop system with the same relay amplitude, the output responses have similar amplitudes and frequency.

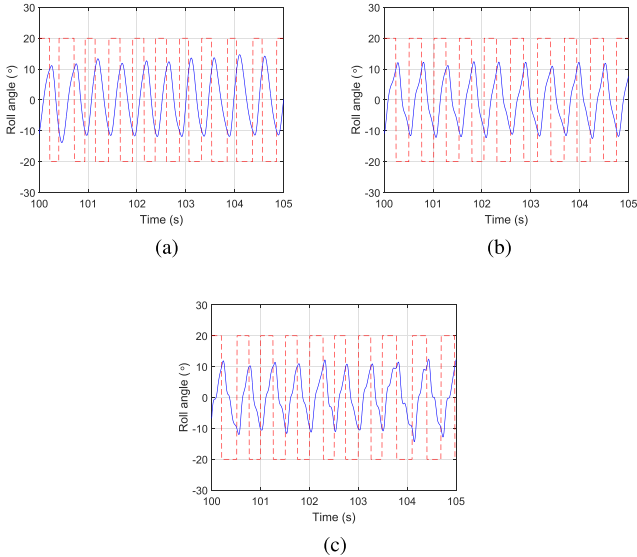


Fig. 7. Outer loop relay results. Dashed lines: relay reference. Solid lines: roll rate feedback. (a) Minimum flight speed (7 m/s). (b) Operational cruise speed (10 m/s). (c) Maximum flight speed (15 m/s).

TABLE V
IDENTIFIED OUTER LOOP CONTROLLER PARAMETERS

	K_{c2}	τ_{I2}
Low speed	7.38	23.2
Medium speed	7.67	24.12
High speed	8	24.2

The performance factor β is selected as 8, as the outer loop of a cascade control system should have a slower closed-loop response. The gain and phase margins corresponding to the integral time delay model are then calculated to be approximately 6.6 and 63°, respectively. From Table V, the calculated controller parameters for each operating point are very close to each other. This is because the inner loop has been tuned in such a way that its response has the same specified performance in a wide range of conditions. This means the outer loop does not require gain scheduling, because it will not have a significant effect on the performance. Therefore, the outer loop PI controller is not scheduled in this paper, and the controller gains are selected from the medium operating condition.

V. PERFORMANCE EVALUATION

In this section, the performance of the automatically tuned PI controller with and without gain scheduling is compared using step response and zero reference tests. Subsequently, a wind tunnel flight test is conducted.

A. Conventional Cascaded PI

First, step response and zero reference tests are performed on a conventional cascaded PI control system configured, as shown in Fig. 8. Both inner and outer loop controller gains are chosen by automatically tuning the flight controller at the aircraft's operational cruise speed, where the inner loop PI controller's parameters are $K_{c1} = 0.23$ and $\tau_{I1} = 0.146$ and

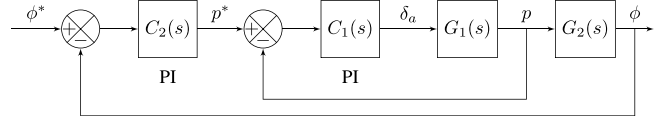


Fig. 8. Cascaded PI control system diagram.

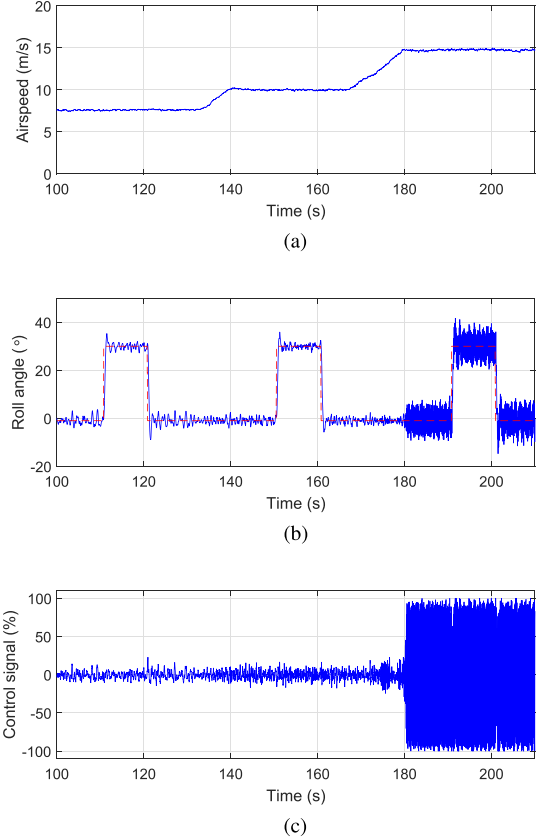
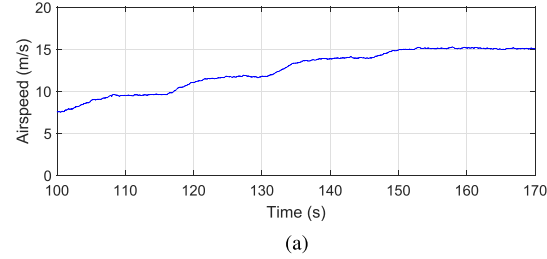


Fig. 9. Conventional cascaded PI step response test. Dashed line: roll angle reference. Solid lines: measured data. (a) Measured airspeed. (b) Conventional PI controller. (c) Roll control signal without gain scheduling.

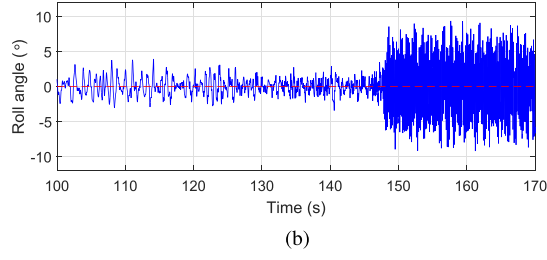
the outer loop controller's parameters are $K_{c2} = 7.67$ and $\tau_{I2} = 24.12$.

Three different operating conditions were used in the testing of the cascaded control system, which was dictated by the changes of the airspeed from 7 to 15 m/s, as shown in Fig. 9(a). For each operating condition, two step reference changes for the roll angle were performed, as shown in Fig. 9(b). It is seen that from the closed-loop system response to the angular reference change becomes oscillatory when the airspeed increases to the higher operating region. Meanwhile, the control signal reaches saturation during the operation. As a consequence, the ailerons actuate at high frequency and amplitude leading to actuator degradation over time.

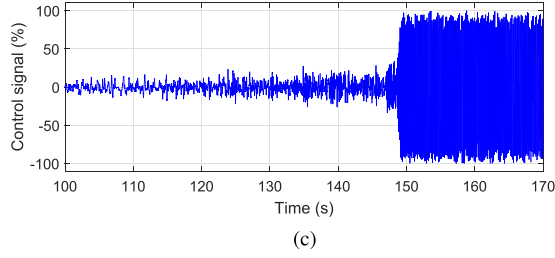
The second set of the experiments was conducted in the environment where the airspeed was changed gradually as shown in Fig. 10(a). The reference signal for the roll angle was maintained at zero, representing a straight and leveled flight. Fig. 10(b) and (c) shows the closed-loop output and control signal responses. It is seen from Fig. 10(b) and (c) that as the airspeed gradually increases, the closed-loop control system



(a)

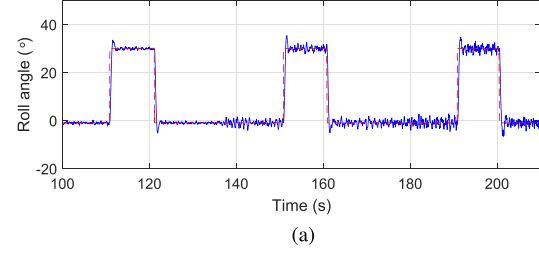


(b)

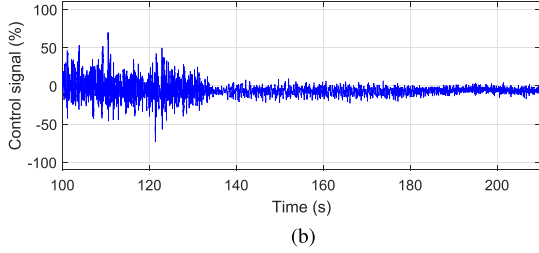


(c)

Fig. 10. Conventional cascaded PI zero reference test with wind speed variation. Dashed line: roll angle reference. Solid lines: measured data. (a) Measured airspeed. (b) Conventional PI controller. (c) Roll control signal without gain scheduling.



(a)

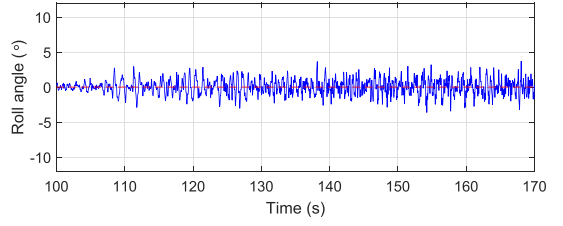


(b)

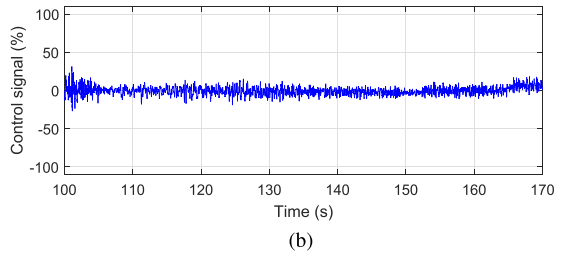
Fig. 11. Gain scheduled cascaded PI step response test. Dashed lines: roll angle reference. Solid lines: measured data. (a) Gain scheduled PI controller. (b) Roll control signal with gain scheduling.

becomes oscillatory. Again, the ailerons reach their maximum deflection angles with high frequency oscillation.

These experimental results confirm the importance of using gain scheduling control strategy for fixed-wing UAVs because of the nonlinearities due to variations of the airspeed.



(a)



(b)

Fig. 12. Gain scheduled PI zero reference test with wind speed variation. Dashed line: roll angle reference. Solid lines: measured data. (a) Gain scheduled PI controller. (b) Roll control signal with gain scheduling.

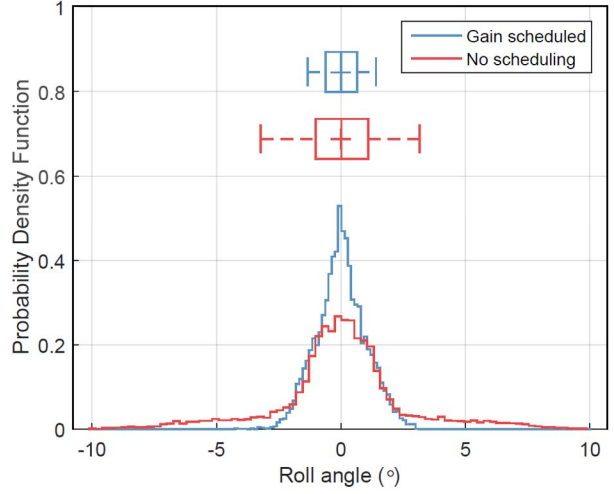


Fig. 13. Roll angle probability density function.

B. Gain Scheduled Cascaded PI

For the gain scheduled system, the controller architecture is configured as shown earlier in Fig. 2, and the inner loop controller used is a gain scheduled PI with parameters from Table IV, while the outer loop controller is a time-invariant PI controller with $K_{c2} = 7.67$ and $\tau_{12} = 24.12$.

The step response and zero reference experimental results are shown in Figs. 11 and 12. The experiments were performed while replicating the airspeeds of the experiments conducted on the conventional cascaded PI system. Based on the results obtained, the gain scheduled system clearly outperforms the conventional cascaded PI control system. In both cases, the roll angle deviation from the reference is smaller at low speed. At high speed, the output does not oscillate, while the control signal is kept relatively low. Thus, it is clear that the gain scheduled control system is necessary to achieve stable closed-loop operation. In addition, the aileron deflection in both cases does not reach saturation, which reduces the workload on the actuators.

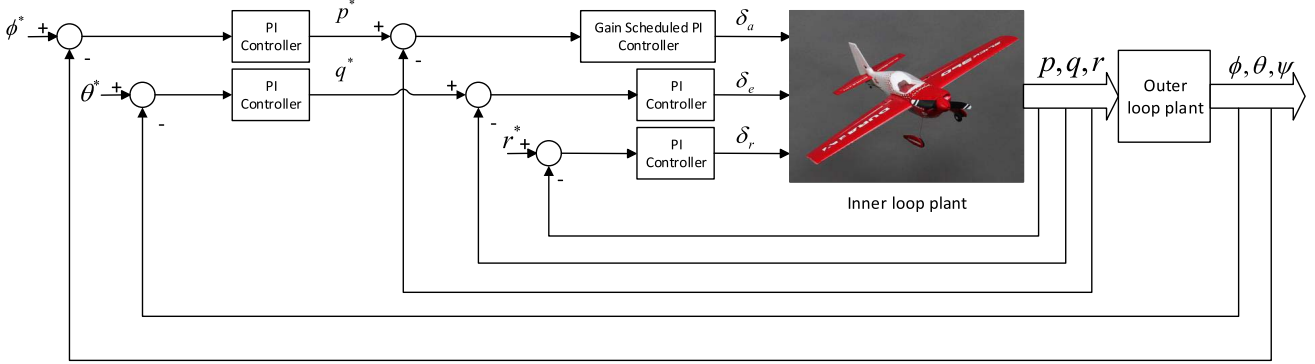


Fig. 14. Flight control system architecture of the UAV.

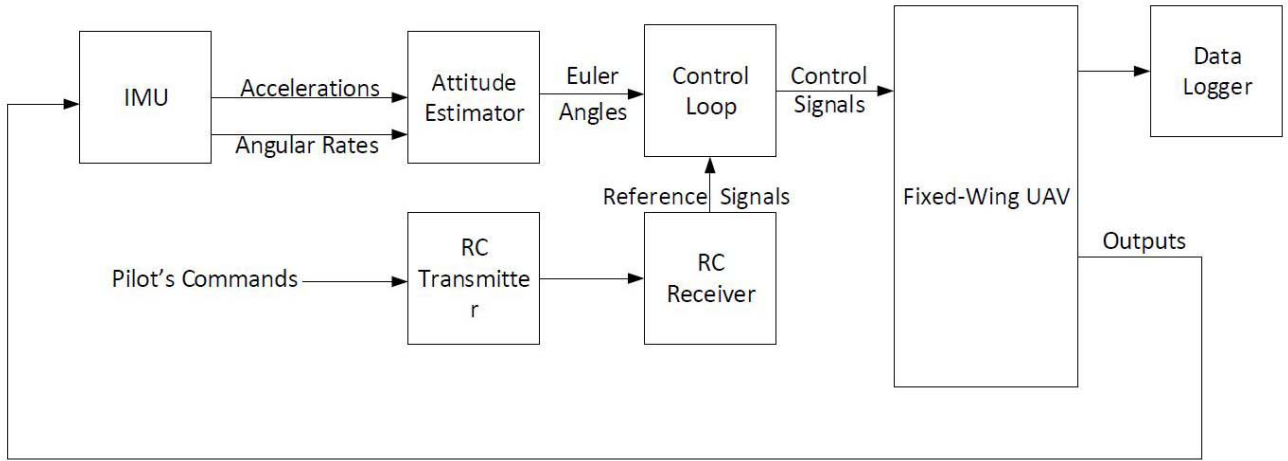


Fig. 15. Custom developed flight controller structure.

Boxplots and histograms are commonly used to display the variations in the attitude data [38]. Fig. 13 shows the histograms of the density estimation of distribution of the roll angle from the zero reference tests for the PI control systems with and without gain scheduling mechanism. The boxplots illustrate the spread and skewness of the standard deviations. Based on the data probability density function, the gain scheduled system has a lower standard deviation and higher peak, implying that the gain scheduled cascaded PI control system has smaller deviation from the reference signal.

C. Tethered Wind Tunnel Flight Test

To replicate cruising flight conditions, a wind tunnel flight test is conducted. Although only the automatic tuning of roll angular controller is presented, a full multi-input–multioutput (MIMO) controller was developed for the aircraft. The pitch and yaw axes were tuned in a similar manner. The control system architecture of the full MIMO structure is shown in Fig. 14.

The flight control system structure is shown in Fig. 15. The control loop starts with the microprocessor receiving the linear accelerations and angular rates from the inertial measurement unit, which are then used to estimate the aircraft's attitude. The reference signals are imposed by the pilot's command via RC receiver/transmitter. Subsequently, the servos are

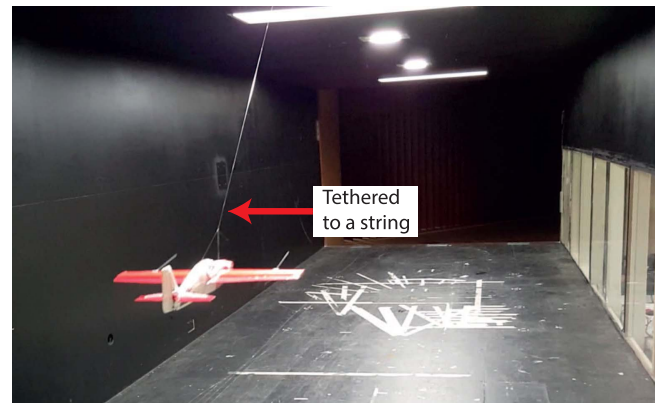


Fig. 16. Wind tunnel flight test setup.

actuated based on the calculated control signals. Meanwhile, the datalogger continuously records the flight data for postanalysis.

For this flight experiment, the UAV is tethered to a string at its center of gravity, as shown in Fig. 16. The UAV was flown in the test section of the wind tunnel, while the wind speed is randomly adjusted. The data are collected while the aircraft is airborne. The data while the string is fully stretched are neglected, since it will induce undesirable accelerations.

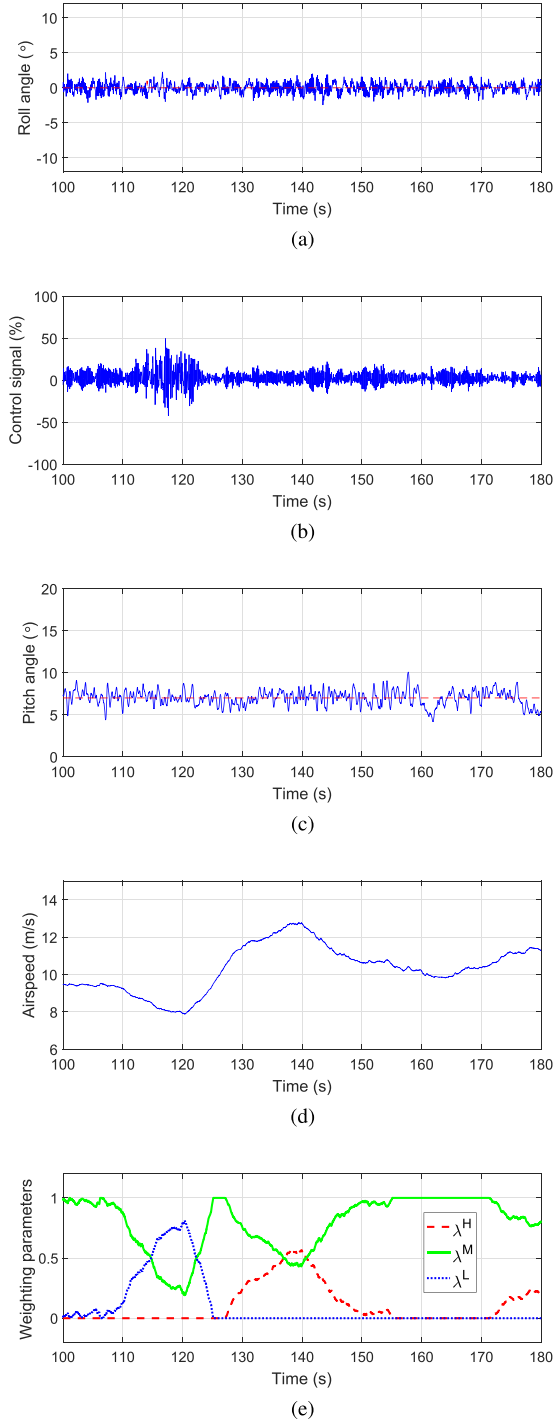


Fig. 17. Wind tunnel flight test results. Dashed lines: angle references. Solid lines: measured data. (a) Roll angle tracking. (b) Roll control signal. (c) Pitch angle tracking. (d) Measured airspeed. (e) Weighting parameters.

Fig. 17 presents the experimental results of the tethered wind tunnel flight test. The roll angle reference signal is maintained at zero, so that the plane is constantly flying into the wind, representing straight and level flight. The reference signal for the pitch angle is kept at its equilibrium. It is seen from Fig. 17(a) and (c) that the roll and pitch angles are regulated closely to their respective reference signals. Fig. 17(d) shows the airspeed measured by the on-board pressure sensors, where the speed was randomly adjusted to replicate outdoor

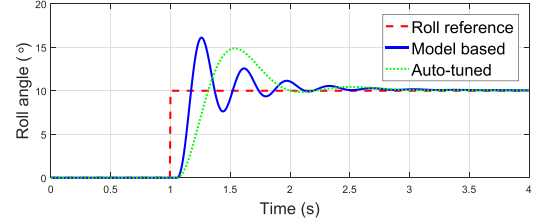


Fig. 18. Comparison between model-based designed and automatically tuned systems.

flying conditions. The weighting parameters were calculated online with respect to Fig. 4, where the boundary parameters are $V_a^L = 7 \text{ m/s}$, $V_a^M = 10 \text{ m/s}$, $V_a^H = 15 \text{ m/s}$, and $\delta = 1$. The calculated weighting parameters are presented in Fig. 17(e), and it is seen that the parameters change with respect to the change in airspeed. For instance, during high speed flight between $t = 130$ and $t = 150$, $\lambda^L = 0$ while λ^M and λ^H vary accordingly. It is clear that the aircraft is able to fly in varying airspeed, which validates the robustness of the automatic tuning algorithm for the gain scheduled controller. The flight data of the wind tunnel flight test with linear PI controllers are not included as it became unstable in varying wind conditions; therefore, a successful flight test could not be achieved. This confirms that gain scheduling is required for fixed-wing UAVs to maintain stability in varying wind speeds.

D. Simulation Comparison With Physical Model-Based Design

A simulation study has been performed to compare the performance of the autotuner with the traditional model-based design presented in [31]. Both controllers were designed with the same requirements where the controller gains for the model-based approach were calculated using the physical parameters of the aircraft, but the actuator dynamics were neglected. Fig. 18 shows the comparative results of the closed-loop step responses where a step change is induced at $t = 1 \text{ s}$. It is seen that the model-based design produces oscillatory closed-loop response due to the unmodeled actuator dynamics. In contrast, the autotuner has produced a closed-loop response that satisfies the original design requirements.

VI. CONCLUSION

There are various issues associated with designing gain scheduled controllers for fixed-wing UAVs. Therefore, this paper proposes an automatic tuning approach to tune systems with nonlinear dynamics based on the relay feedback experiment. Relay tests were performed on a small fixed-wing UAV at different operating points to systematically identify appropriate controller gains that will satisfy the design requirements. The automatically tuned gain scheduled controller is then validated through a series of wind tunnel tests, which include step response, zero reference, and a wind tunnel flight test with wind speed variation. By using the proposed method, the attitude deviation from the reference is clearly lower than the conventional control architecture. It is also apparent that the control signals are not saturated, thus preventing actuator degradation in addition to implying higher efficacy. This shows that improved performance has been achieved with the

automatically tuned gain scheduled controller. To improve the flight performance even further, research on gain scheduling with angle-of-attack as the scheduling parameter is subject to future research.

ACKNOWLEDGMENT

The authors would like to thank the technical support provided by G. Atkins at RMIT University for setting up the experimental instruments in order to conduct the presented research. They would also like to thank the Australian Government for supporting this research through the Australian Government Research Training Program Scholarship. This research was undertaken as a part of the RMIT Unmanned Aircraft Systems Research Team, within the Sir Lawrence Wackett Aerospace Research Centre, RMIT University.

REFERENCES

- [1] R. W. Beard *et al.*, "Autonomous vehicle technologies for small fixed-wing UAVs," *J. Aerosp. Comput., Inf., Commun.*, vol. 2, no. 1, pp. 92–108, 2005.
- [2] M. Elbanhawi, A. Mohamed, R. Clothier, J. L. Palmer, M. Simic, and S. Watkins, "Enabling technologies for autonomous MAV operations," in *Proc. Progr. Aerosp. Sci.*, Mar. 2017, pp. 1–26. [Online]. Available: <http://dx.doi.org/10.1016/j.paerosc.2017.03.002>
- [3] S. Watkins, A. Mohamed, A. Fisher, R. Clothier, R. Carrese, and D. Fletcher, "Towards autonomous MAV soaring in cities: CFD simulation, EFD measurement and flight trials," *Int. J. Micro Air Veh.*, vol. 7, no. 4, pp. 441–448, 2015.
- [4] A. Mohamed, R. Carrese, D. F. Fletcher, and S. Watkins, "Scale-resolving simulation to predict the updraught regions over buildings for MAV orographic lift soaring," *J. Wind Eng. Ind. Aerodyn.*, vol. 140, pp. 34–48, May 2015. [Online]. Available: <http://dx.doi.org/10.1016/j.jweia.2015.01.016>
- [5] C. White, E. Lim, S. Watkins, A. Mohamed, and M. Thompson, "A feasibility study of micro air vehicles soaring tall buildings," *J. Wind Eng. Ind. Aerodyn.*, vol. 103, pp. 41–49, Apr. 2012.
- [6] A. Mohamed, S. Watkins, R. Clothier, M. Abdulrahim, K. Massey, and R. Sabatini, "Fixed-wing MAV attitude stability in atmospheric turbulence—Part 2: Investigating biologically-inspired sensors," *Progr. Aerosp. Sci.*, vol. 71, pp. 1–13, Nov. 2014.
- [7] A. Mohamed, S. Watkins, R. Clothier, M. Abdulrahim, K. Massey, and R. Sabatini, "Fixed-wing MAV attitude stability in atmospheric turbulence, part 1: Suitability of conventional sensors," *Progr. Aerosp. Sci.*, vol. 70, pp. 69–82, Oct. 2014.
- [8] A. Mohamed, K. Massey, S. Watkins, and R. Clothier, "The attitude control of fixed-wing MAVs in turbulent environments," *Progr. Aerosp. Sci.*, vol. 66, pp. 37–48, Apr. 2014.
- [9] M. Euston, P. Coote, R. Mahony, J. Kim, and T. Hamel, "A complementary filter for attitude estimation of a fixed-wing UAV," in *Proc. IEEE/RSJ Int. Conf. Intell. Robots Syst. (IROS)*, Sep. 2008, pp. 340–345.
- [10] A. Mystkowski, "Robust Control of the micro UAV dynamics with an autopilot," *J. Theor. Appl. Mech.*, vol. 51, no. 3, pp. 751–761, 2013.
- [11] M. Abdulrahim, A. Mohamed, and S. Watkins, "Control strategies for flight in extreme turbulence," in *Proc. AIAA Guidance, Navigat. Control Conf.*, 2017, p. 1909. [Online]. Available: <http://arc.aiaa.org/doi/10.2514/6.2017-1909>
- [12] J.-M. Biannic, P. Apkarian, and W. L. Garrard, "Parameter varying control of high-performance aircraft," *J. Guidance, Control, Dyn.*, vol. 20, no. 2, pp. 225–231, 1997.
- [13] L. Ravanbod and D. Noll, "Gain-scheduled two-loop autopilot for an aircraft," *J. Dyn. Syst., Meas., Control*, vol. 136, no. 4, p. 041021, 2014.
- [14] J. Wang and N. Sundararajan, "A nonlinear flight controller design for aircraft," *Control Eng. Pract.*, vol. 3, no. 6, pp. 813–825, 1995.
- [15] W. J. Rugh, "Analytical framework for gain scheduling," in *Proc. Amer. Control Conf.*, 1990, pp. 1688–1694.
- [16] N. V. Hoffer, C. Coopmans, A. M. Jensen, and Y. Chen, "A survey and categorization of small low-cost unmanned aerial vehicle system identification," *J. Intell. Robot. Syst., Theory Appl.*, vol. 74, no. 1, pp. 129–145, 2014.
- [17] E. M. Jafarov, "H inf. Loop shaping robust control vs. classical PI (D) control: A case study on the longitudinal dynamics of hezarfen UAV," in *Proc. 2nd WSEAS Int. Conf. Dyn. Syst. Control*, 2006, pp. 105–110.
- [18] B. Kada and Y. Ghazzawi, "Robust PID controller design for an UAV flight control system," in *Proc. World Congr. Eng. Comput. Sci.*, vol. 2, 2011, pp. 1–6.
- [19] Y. Luo, H. Chao, L. Di, and Y. Chen, "Lateral directional fractional order (PI) π control of a small fixed-wing unmanned aerial vehicles: Controller designs and flight tests," *IET Control Theory Appl.*, vol. 5, no. 18, p. 2156, 2011.
- [20] M. Ahsan, K. Rafique, and F. Mazhar, "Optimization based tuning of autopilot gains for a fixed wing UAV," *World Academy Sci., Eng. Technol., Int. J. Mech., Aerospace, Ind., Mech. Manuf. Eng.*, vol. 7, no. 5, pp. 1–6, 2013.
- [21] P. Poksawat, L. Wang, and A. Mohamed, "Automatic tuning of attitude control system for fixed-wing unmanned aerial vehicles," *IET Control Theory Appl.*, vol. 10, no. 17, pp. 2233–2242, 2016.
- [22] K. J. Astrom, "PID controllers: Theory, design, and tuning," in *Instrument Society of America*. Asheville, NC, USA: ISA Research Triangle Park, 1995.
- [23] K. J. Astrom and T. Hagglund, *Automatic Tuning of PID Controllers*. Instrument Society of America (ISA), 1988.
- [24] T. Hagglund and K. J. Astrom, "Method of an apparatus in tuning a PID-regulator," U.S. Patent 4 549 123, 1985.
- [25] K. J. Astrom and T. Hagglund, *Advanced PID Control*. ISA-The Instrumentation, Systems and Automation Society, 2006.
- [26] M. A. Johnson and M. H. Moradi, *PID Control New Identification and Design Methods*. London, U.K.: Springer, 2005.
- [27] C. C. Yu, *Autotuning of PID Controller: A Relay Feedback Approach*. London, U.K.: Springer, 2006.
- [28] A. Visioli and Q. Zhong, *Control of Integral Processes With Dead Time*. London, U.K.: Springer, 2010.
- [29] L. Wang, *Model Predictive Control System Design and Implementation Using MATLAB*. London, U.K.: Springer, 2009.
- [30] L. Wang, S. Chai, D. Yoo, L. Gan, and K. Ng, *PID and Predictive Control of Electrical Drives and Power Converters*. New York, NY, USA: Wiley, 2015.
- [31] R. W. Beard and T. W. McLain, *Small Unmanned Aircraft: Theory and Practice*. Princeton, NJ, USA: Princeton Univ. Press 2012.
- [32] S. A. Salman, A. G. Sreenatha, and J. Y. Choi, "Attitude dynamics identification of unmanned aircraft vehicle," *Int. J. Control., Autom., Syst.*, vol. 4, no. 6, pp. 782–787, 2006.
- [33] C. Desoer, "Slowly varying system $\dot{x} = A(t)x$," *IEEE Trans. Autom. Control*, vol. 14, no. 6, pp. 780–781, Dec. 1969.
- [34] L. Wang and W. R. Cluett, *From Plant Data to Process Control: Ideas for Process Identification and PID Design*. London, U.K.: Taylor & Francis, 2000.
- [35] L. Wang and W. R. Cluett, "Tuning PID controllers for integrating processes," *IEE Proc.-Control Theory Appl.*, vol. 144, no. 5, pp. 385–392, Sep. 1997.
- [36] A. Mohamed, S. Watkins, A. Fisher, M. Marino, K. Massey, and R. Clothier, "A feasibility study of bio-inspired wing-surface pressure sensing for attitude control of micro aerial vehicles," *J. Aircraft*, vol. 52, no. 3, pp. 827–838, 2015.
- [37] A. Mohamed, S. Watkins, R. Clothier, and M. Abdulrahim, "Influence of turbulence on MAV roll perturbations," *Int. J. Micro Air Veh.*, vol. 6, no. 3, pp. 175–190, 2014.
- [38] A. Mohamed, M. Abdulrahim, S. Watkins, and R. Clothier, "Development and flight testing of a turbulence mitigation system for MAVs," *J. Field Robot.*, vol. 33, no. 5, pp. 639–660, 2016.
- [39] S. Ravi, "The influence of turbulence on a flat plate aerofoil at Reynolds numbers relevant to MAVs," Ph.D. dissertation, Dept. Mech. Manuf. Eng., RMIT Univ., Melbourne, VIC, Australia, 2011.



Pakorn Poksawat received the B.Eng. degree (Hons) in electrical engineering from RMIT University, Melbourne, VIC, Australia, in 2014, where he is currently pursuing the Ph.D. degree, sponsored by the Australian Government Research Training Program Scholarship.

His current research interests include proportional-integral derivative control systems, model predictive control, and fixed-wing and multirotor unmanned aerial vehicles.

Mr. Poksawat received the Vice-Chancellor's List for Academic Excellence Award for achieving academic results in the top 2% of RMIT higher education students in 2014.



Liuping Wang received the Ph.D. degree from The University of Sheffield, Sheffield, U.K.

She was with the University of Toronto, Toronto, ON, Canada, for eight years in the field of process control. From 1998 to 2002, she was with The University of Newcastle, Callaghan, NSW, Australia. In 2002, she joined RMIT University, Melbourne, VIC, Australia, where she is currently a Professor of Control Engineering. She has authored or co-authored over 190 scientific papers in systems and control. She co-authored a book with Prof. Cluett *From Process Data to Process Control: Ideas for Process Identification and PID Control* (Taylor and Francis, 2000). She co-edited two books with Prof. Garnier *Continuous Time Model Identification From Sampled Data* (Springer-Verlag, 2008) and *System Identification, Environmental Modelling and Control* (Springer-Verlag, 2011). She authored the book *Model Predictive Control Design and Implementation Using MATLABR* (Springer-Verlag, 2009). She is the Lead Author of the book *PID and Predictive Control of Electrical Drives and Power Converters Using MATLABR* (Wiley-IEEE, 2015).



Abdulghani Mohamed received the Ph.D. degree in aerospace engineering from RMIT University, Melbourne, VIC, Australia.

He has successfully made some noteworthy contributions to aeronautical engineering. He has developed the world's most stable Micro Air Vehicle through inventing and patenting a novel biomimetic sensor inspired by birds. His research has significant impact with respect to enabling safer and more efficient flight of aircraft in turbulent weather. He is a multidisciplinary Researcher involved in a number of areas, such as robotics, aerodynamics, turbulence, biomimetics, sensors, dynamics, and control. His current research interests include numerous media outlets, such as scientific magazine articles, interviews on radio and TV, and videos that have attracted a significant view count on social media websites.

Dr. Mohamed received a number of awards, including the prestigious 2015 Young Innovators Award.